Composites Science and Technology 262 (2025) 111084

Contents lists available at ScienceDirect

Composites Science and Technology

journal homepage: www.elsevier.com/locate/compscitech

Quantitative analysis of orientation distribution of graphene platelets in nanocomposites using TEM

Osman Bayrak [a], Mikhail Tashkinov [b], Vadim V. Silberschmidt [c,*], Emrah Demirci [c]

[a] Mechanical Engineering Department, Bursa Technical University, 16310, Bursa, Turkiye
[b] The Laboratory of Materials and Structures with Embedded Intelligence, Perm National Research Polytechnic University, 29 Komsomolsky Ave., 614990, Perm, Russia
[c] Wolfson School of Mechanical, Electrical and Manufacturing Engineering, Loughborough University, LE11 3TU, Leicestershire, UK

ARTICLE INFO

Keywords:
Graphene
Nanocomposites
Mechanical behavior
Transmission electron microscopy
Spatial orientation
Finite-element modelling

ABSTRACT

Mechanical properties of nanocomposites are directly affected by their microstructures. Orientation distribution of nano-reinforcements, one of the critical microstructural parameters, is, therefore, of great importance. However, methods to quantify their orientation are limited. Many studies employ transmission electron microscopy (TEM) for qualitative characterisation of orientation distribution of graphene nanoplatelets (GNPs) in nanocomposites. However, there is no report in the literature that does it quantitatively based on TEM micrographs. In this study, a method for the use of TEM in quantitative characterisation of the orientation distribution of GNPs in nanocomposites is suggested. Materials used for this purpose were sodium alginate nanocomposites reinforced with GNPs. In order to assess the effectiveness of the suggested method, finite-element (FE) models of representative volume elements (RVEs) of the nanocomposites were developed based on the GNPs' orientation distribution data. Elastic-range tensile tests of these composites were simulated with the RVEs. The simulation results were compared with the data from experiments reported in our previous study. A strong correlation between the obtained results of numerical simulations and the experimental data was observed. Young's moduli of the nanocomposites, calculated with the simulations, were slightly higher than those from the experiments. A discrepancy of less than 4 % in the Young's moduli can be attributed to other microstructural parameters such as spatial distribution nonuniformity, wrinkling and dimensional variation of the GNPs, which were not taken into account in the FE models. Some micromechanical models were also implemented in order to assess their capability to predict the effect of GNP orientation distributions on stiffness of the nanocomposites. The Krenchel orientation factors were incorporated into the models for this purpose. This study shows that the quantitative characterisation of orientation distribution of graphene in nanocomposites is achievable through TEM analyses with the suggested methodology and can be used to underpin analysis of their properties and performance.

1. Introduction

Microstructural features affect almost all physical properties of composites, such as mechanical, thermal, electrical, optical, etc. Characterisation of microstructure is a critical stage for development of many types of composites systems reinforced with novel nanofillers like graphene-based materials [1–3]. Orientation distribution of reinforcements is one of the most important microstructural features of composites [4]. Various studies showed that orientation distribution of graphene played a key role in determining mechanical properties of nanocomposites [5–8]. Orientation of graphene nanoplatelets parallel to the main plane of nanocomposites improves their in-plane Young's modulus compared to the cases with randomly aligned GNPs [7]. Orientation of GNPs is influenced by manufacturing methods of nanocomposites [9], and by the types of materials used [10]. Therefore, together with available manufacturing methods and types of materials, a quantitative characterisation method would help to control orientation distribution of GNPs in nanocomposites, and, hence, tailor their properties.

Methods used for characterisation of orientation distribution of the GNPs in nanocomposites are diverse, such as optical microscopy (OM) [11,12], X-ray diffractometry (XRD) [13], Raman spectroscopy [5], scanning electron microscopy (SEM) [9], and transmission electron microscopy (TEM) [14]. However, most of these methods are used for

* Corresponding author.
E-mail address: v.silberschmidt@lboro.ac.uk (V.V. Silberschmidt).

https://doi.org/10.1016/j.compscitech.2025.111084
Received 24 April 2024; Received in revised form 22 January 2025; Accepted 27 January 2025
Available online 28 January 2025

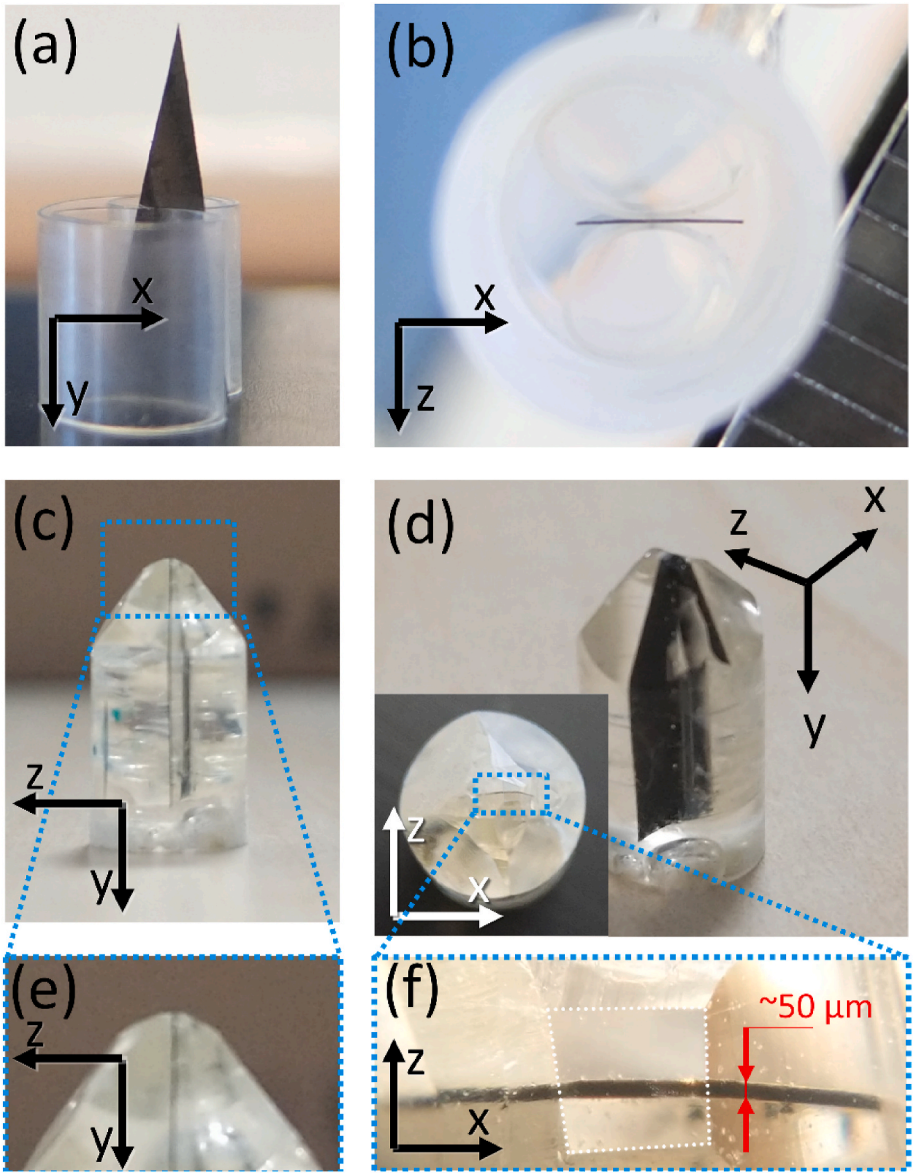

Fig. 1. Sample-preparation stages for ultramicrotome sectioning: (a) placement of pointed sample in mounting clip (plane of nanocomposite film is x-y plane); (b) positioning of clip-mounted sample in BEEM® capsule (through-thickness direction is z-axis); (c) sample in resin mould in y-z plane; (e) detail of sample tip in y-z plane; (d) isometric view of resin block and film; (f) microscopic image of tip of sectioned block.

qualitative analyses of the reinforcement distribution. Due to its low resolution, optical microscopy can analyse the orientation distribution of nanoplatelets not through-thickness but in-plane [11,12]. This is because the thickness of the GNPs is in the nanometres range while their planar dimensions are at micrometres range. This does not allow OM to characterise nanoplatelets' orientation distribution, but only their planar distribution. X-ray diffractometry (XRD) [13] was used to obtain an average orientation degree for graphite platelets, while Raman spectroscopy was employed for quantitative characterisation of orientation distribution of GNPs in nanocomposites [15,16]. Obtaining an orientation distribution function (ODF) with Raman spectroscopy, Li et al. [5] studied the effect of the orientation distribution on the Young's moduli of the nanocomposites.

Thanks to the high-resolution capability of the electron microscopy instruments, SEM and TEM studies allow the characterisation of orientation distribution of nanoplatelets also in the thickness direction. SEM was used for a quantitative characterisation of the orientation distribution of GNPs in ceramic matrix nanocomposites [9]. One drawback of this study is that it did not directly relate the orientation distributions to the planes of nanocomposites: it assumed all micrographs to be oriented at 45° to the plane of the nanocomposites and calculated the orientation distributions accordingly. So far, TEM was employed only for a qualitative characterisation of orientation distribution of graphene nanoplatelets [6,13,14]. Defining a reference axis for a sectioned sample in TEM is difficult: one reason is that an orientation-controlled transfer of freely floating sections onto TEM grids is almost impossible. Still, position-controlled sample preparation can be made possible with a focused-ion beam (FIB) technique; however, this may lead to FIB-related damage of samples [17]. Another reason is the nature of the spiral path that the electron beam follows. Due to such path, image rotations occur as the magnification is altered [18]. With advances in electromagnetic lenses, the unwanted rotations can be compensated [19]. However, the image rotations can still occur during focusing on images [20]. Uncontrollable rotations prevent the detection of reference axes (or planes) of the observed samples. Even though image rotations can be prevented, the detection of reference planes or reference axes can still be difficult. This is because thin sections of samples may degrade due to electron-beam damage [21], which can also make through-thickness or

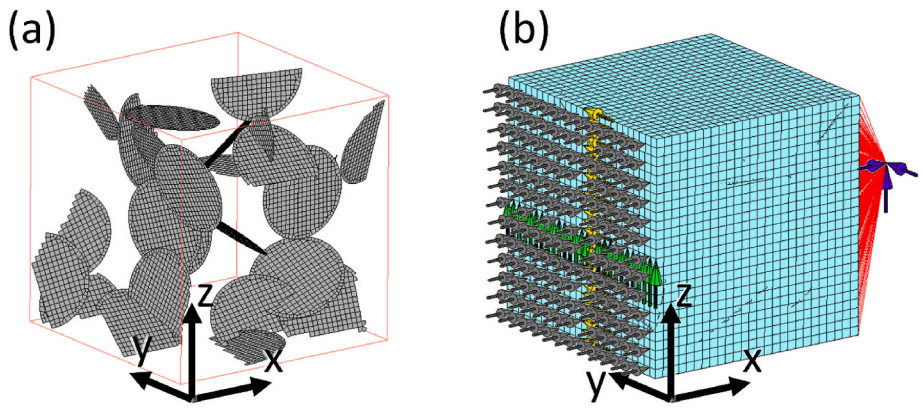

Fig. 2. (a) RVE of nanocomposite with GNPs (protruding areas of GNPs were trimmed). (b) FEM of nanocomposite showing BCs. (The grey vectors were partially hidden in order to allow clear view of the fixing in z and y directions) RVE's edge size is 5.3 μm.

Table 1
Young's modulus (E), Poisson's ratio (ν), element types, and geometric parameters of FE models.

	Young's modulus (GPa)	Poisson's ratio	element type	geometrical parameters
GNP	85.7	0.28	4-node shell	t: 25 nm, d: 2 μm
Matrix	4.75	0.4	8-node hexahedral	–

(t -thickness, d - diameter).

planar directions of the sections ambiguous. Therefore, characterisation of the orientation distribution of nanoparticles cannot be done quantitatively with traditional TEM imaging methods.

This study suggests a novel imaging methodology with TEM for a quantitative characterisation of orientation distribution of graphene in nanocomposites: the respective procedure for preparation of samples for TEM and approaches for analysis of micrographs were defined. The obtained micrographs were processed to obtain the orientation distribution of GNPs using a custom-made image processing software (Nonwovens Anisotropy V1, developed by Demirci et al. [22] in MatLab), originally designed for detection and characterisation of orientation of fibres in nonwoven materials. As a result, ODFs of graphene nanoplatelets were determined. In order to assess the validity of the suggested methodology, the finite-element (FE) method was employed. FE models of the nanocomposites were developed based on the orientation distribution data obtained from this study and additional geometrical data presented in a previous study [14]. Numerical simulations of tension of composites with nanofillers were performed with the developed FE models. Young's moduli obtained from the simulation results were compared with those from experiments presented in Ref. [14]. The effect of orientation distribution was also assessed with micromechanical models. In order to achieve this, Krenchel's orientation factors [5,23] of the nanocomposites were calculated and incorporated into these models employing the modified rule of mixtures, Halpin-Tsai, and Hui-Shia approaches [11].

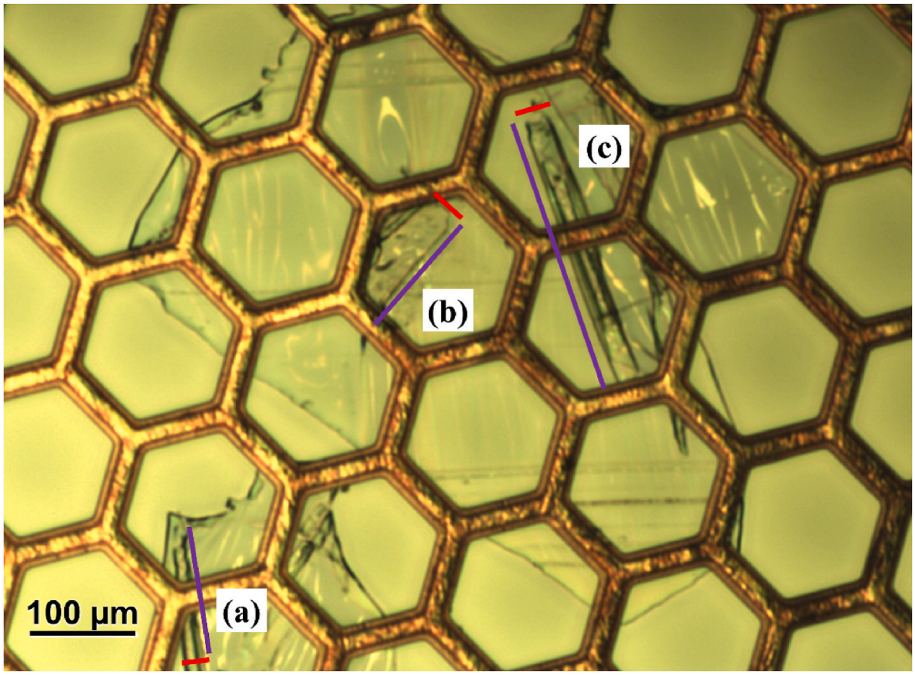

Fig. 3. Appearance of sections under optical microscope (red lines represent z-axis and purple lines represent x-axis of sections). The degree of detachment of the sections from the surrounding resins is higher for sections (a) and (c) and lower for section (b). The detachment leads to artefacts of fold-overs and wrinkles. Therefore, the higher the level of detachment, the smaller the thickness (the z-direction) of the sections. The fold-overs (dark lines) are usually parallel to the x-axis.

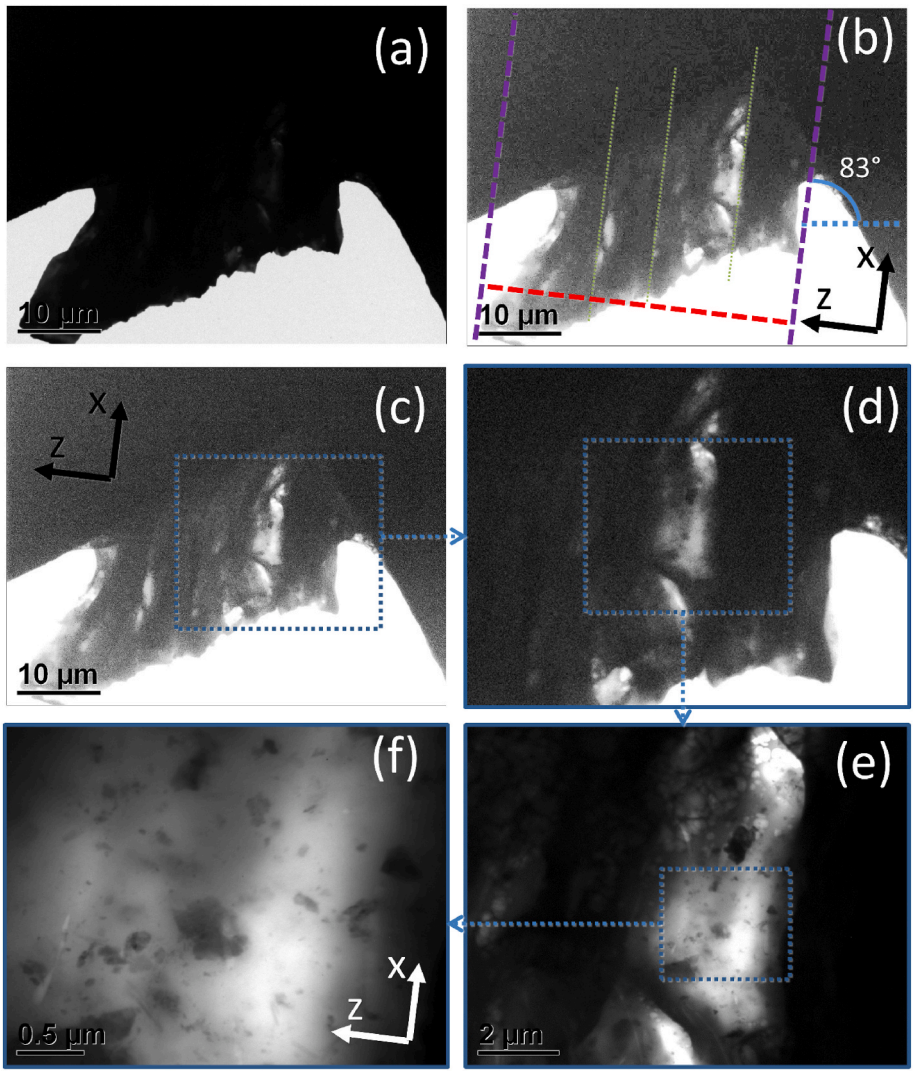

Fig. 4. Coordinate assignment for sections in micrographs: (a) original TEM image of section of 1.0 wt% GO-SA nanocomposite; (b) image edited with brightening of original for focused area and artefacts appear clearly. (The thin green lines highlight the fold-overs, the purple lines show the top and bottom plane edges, and the red line shows the through-thickness direction.) (c), (d), and (e) respective magnified areas. (f) smallest-scale micrograph with GNPs.

2. Experimental and modelling details

2.1. Sample preparation and characterisation

Manufacturing methods of graphene oxide (GO)-reinforced sodium alginate (GO-SA) nanocomposites were described by Ionita et al. in Ref. [24]. The nanocomposites used in our study were manufactured in the form of flat films with ~50 μm thickness. Two different concentrations of GO nanoplatelets were used - 1.0 wt% and 2.5 wt%. It was established in Ref. [14] that the GO sheets were dispersed with a morphology of intercalated structures rather than of a single layers. Obviously, taking the morphology of the reinforcements into account is crucial when modelling the nanocomposites. Based on the geometrical and density data presented in Ref. [14], volume fractions of the intercalated structures of GO were calculated as 1.04 vol% and 2.63 vol% for 1.0 wt% and 2.5 wt% nanocomposites, respectively. In this study, the GO flakes with intercalated morphologies are denoted GNPs. In the numerical simulations reported below, mechanical and geometrical properties as well as volume fractions of GNPs are taken into account rather than those of GOs.

For preparation of specimens, small pieces with pointed tips were cut out of the nanocomposite films. The pieces were flat when they were free of external forces. Embedding of the cut samples into BEEM® capsules was carefully performed. The samples were first mounted in a roll-like plastic clips so that they could stand straight within the capsules (see Fig. 1 (a)). The clip-mounted samples were placed inside the capsules, ensuring that the planes of the films were parallel to the longitudinal axis of the capsules (see Fig. 1 (b)). A special attention was paid to the tip for the parallelism. A resin and a hardener were mixed in a container, with the mixture poured into the capsules. The BEEM® capsules were positioned with the tips facing down for the air bubbles to escape from the tips. The epoxy-filled capsules were left for curing at room temperature overnight. The cured moulds taken out of the capsules had well positioned samples embedded in them (see Fig. 1(c) and (d)). The plane and cross-sections of the nanocomposites were assigned the coordinate axes: the plane of the films as parallel to the x-y plane (see Fig. 1(d) and (e)). This ensured that the ultramicrotomy sectioning would occur on x-z plane (see Fig. 1 (f)).

The tips of the moulds were trimmed down to a state with a slender rectangular geometry, i.e., with a large aspect ratio of the lateral size to thickness. This allowed a distinction between x and z axes of the sections. Ultramicrotomy sectioning (instrument used: PC PowerTome, RMC Products®) of the moulds was performed with a diamond trimming knife at a speed of 0.7 mm/s; 85 nm-thick sections were obtained. As the

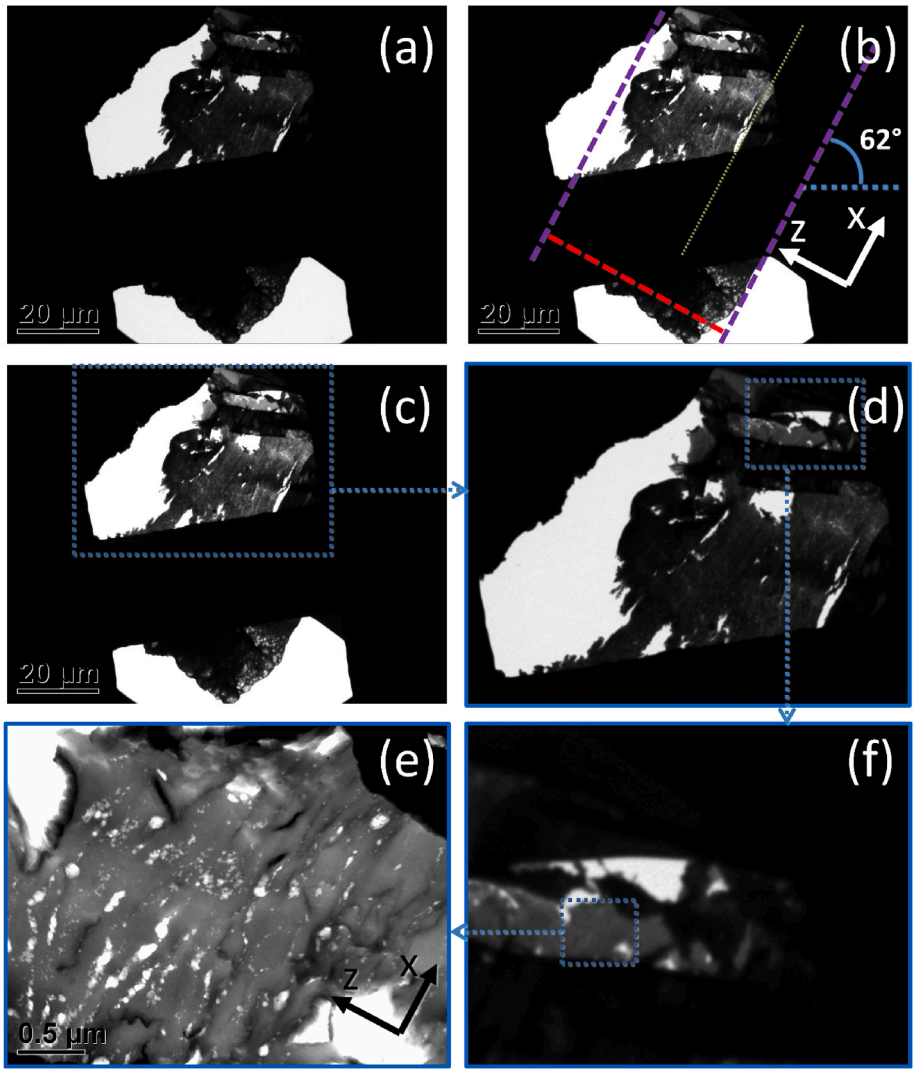

Fig. 5. Coordinate assignment for sections in micrographs: (a) original TEM image of section of 2.5 wt% GO-SA nanocomposite; (b) image edited with brightening of original for focused area and artefacts appear clearly. (The thin green lines highlight the fold-overs, the purple lines show the top and bottom plane edges, and the red line shows the through-thickness direction.) (c), (d), and (e) respective magnified areas. (f) smallest-scale micrograph with GNPs.

matrix material (SA) of the nanocomposites was water-soluble, the sections floated on propanol and transferred onto copper grids.

The morphology of the obtained sections was observed with OM in a transmitted illumination mode. Overall artefacts of the sections were noted. The copper grids with the sections of acceptable quality were selected for the TEM study, conducted with a JEOL® JEM-2000FX transmission electron microscope. Two grids were loaded into the specimen holder for each TEM session. In order to keep the radiation damage of the sections to minimum without compromising the resolution, acceleration voltage of the electron beams was set at 100 kV. As magnification beyond 100,000x was not needed, that voltage was sufficient. Starting from the full view of the sections and going down to the details where GNPs started to appear, the micrographs were taken at incremental magnifications. The areas where the GNPs were clearly seen were artefact-free. These areas were chosen for the analysis of orientation distribution. All the obtained incremental micrographs were saved for image-processing.

The digital copies of the micrographs were transformed into an MS PowerPoint document where x-axis (long edge) and z-axis (short edge, or through thickness) of the sections were determined. This assessment was based mainly on the dimensions of the sections, as well as on the direction of the wrinkles and fold-overs where possible. Following the determination of the axes of the sections, the micrographs were rotated around their y-axes in order to make the x-axis horizontal. GNPs, with the cross-section appearing clearly, were marked with straight lines. The marked lines were then analysed using *Nonwovens Anisotropy V1* software in order to produce the orientation-distribution statistics of the GNPs. The working principle of the software is given in detail in Ref. [22].

2.2. Geometrical and finite-element modelling

Representative volume elements (RVEs) of the nanocomposites were developed for numerical simulations based on the experimental data using a generating algorithm that subsequently filled a three-dimensional volume with randomly placed non-intersecting platelets of the predefined sizes. This algorithm was created and implemented in Wolfram Mathematica. The diameter and thickness of the discs were defined as 2 μm and 25 nm, respectively, based on experimental measurements [14]. Orientations of the discs were defined based on the experimentally obtained distribution statistics of GNPs. These distribution data were statistically analysed and fitted to a parametric uniform distribution law. Parameters of this distribution were determined in each case study using embedded optimization algorithms of Wolfram

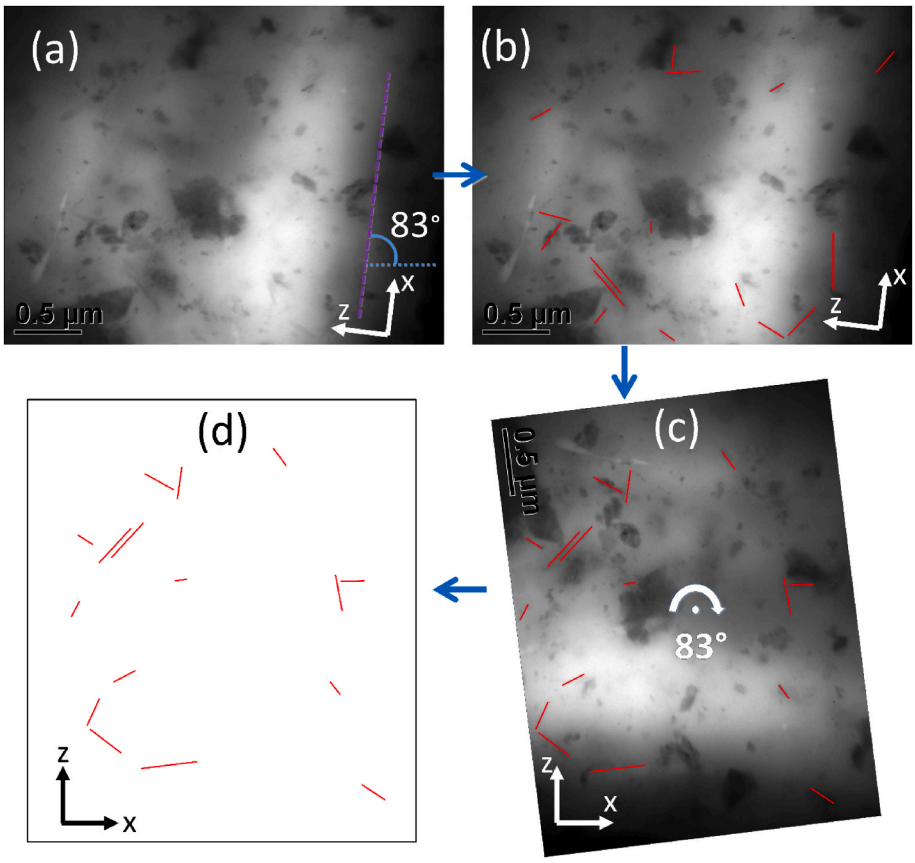

Fig. 6. Stages used for determination and highlighting of GNPs for 1.0 wt% GO-SA nanocomposite.

Mathematica. In order to investigate the effect of the RVE size on mechanical behaviour of the FE models, three different RVEs with edge sizes of 3.1 μm, 5.3 μm, and 7.6 μm were analysed.

Coordinates and orientation data of the discs representing the nanoflakes were transferred into a custom-made Python® code written to run in MSC. Marc® software. FE modelling parameters, such as mesh sizes, boundary conditions (BCs), material definitions, contact features etc., were defined within the code. Once the code was run in MSC. Marc®, the FE models became fully defined, ready for analysis. The parameters also included the RVE size, platelet thickness and material properties. FTIR studies [24] performed on the same nanocomposites indicated a formation of hydrogen bonding between the nanoplatelets and the matrix; therefore, contact between the elements of the two phases in simulations was defined by INSERT operation of the software. This operation ties the degrees of freedom of nearest nodes of the contacting phases, thus simulating the strong hydrogen bonding. Displacement BCs to the RVE faces normal to the x-axis were applied (see Fig. 2).

All the nodes on left-hand face (Fig. 2) were fixed with regard to the x-axis, while the nodes on the right-hand face were tied to a node created outside the RVE. This allowed the transfer of the BCs from the tie node to the nodes of the right face only in the x direction. A displacement-controlled tensile loading was applied: in the x-axis direction, the tie-node was loaded with a displacement of 10 % of the RVE's edge size, so that the RVEs could strain up to 10 % in the positive x direction. In order to avoid a free-body motion of the RVEs, the tie node and the orthogonal midline nodes of the left-hand face were fixed in y and z directions. Mechanical properties of the elements of the matrix and GNPs were defined based on the results presented in Ref. [14]. It is reported in the literature that graphene can be modelled as continuum [25] with finite-elements of linear-elastic mechanical behaviour [26]. In this study, the platelets were modelled as 4-node shell elements with a thickness of 25 nm and the matrix material was meshed with 8-node hexahedral elements. Due to the 6-fold rotational symmetry of graphene and graphene-based materials, these materials have an in-plane isotropic elasticity [27]; hence, graphene is mostly modelled isotropic [28]. The FE models of the GNPs in this study had an aspect ratio of 80 (2000 nm/25 nm), making the effect of through-thickness elastic properties negligible. Therefore, isotropic mechanical properties were defined for both phases. The Young's moduli of pure SA (the matrix) and monolayer GO were reported as 4.75 GPa and 158.7 GPa, respectively, in Ref. [14]. The Young's modulus of monolayer GO was calculated based on its stiffness (~145.3 N m^{-1} [29]) and thickness (~0.916 nm [14]). Also, the respective Poisson's ratios were 0.4 and 0.186. The GNPs in the nanocomposites were in the form of intercalated morphology rather than single sheets of GO. Based on the data reported in Ref. [14], the Young's modulus and Poisson's ratio of the GNPs (the reinforcements) were calculated as 85.7 GPa and 0.28, respectively. Material properties, element types and geometrical parameters employed in the FE models are presented in Table 1. Mesh-size and RVE-size convergence analyses were performed in order to determine the most accurate and the least expensive FE models. In the post-processing stage, the changes of the cross-sectional area (y-z plane) were saved along with the load-displacement data obtained from the tie-node. These collected data were used to plot the true stress-strain curves and calculate the Young's moduli of the nanocomposites.

2.3. Analytical modelling

Analytical micromechanical models are commonly used to optimise the design of composite materials [30]. The Modified Rule of Mixtures (MRoM), Hui-Shia, and Halpin-Tsai schemes are some of the broadly employed micromechanical models [14,31]. In our previous study, those models were adapted for intercalated morphology of the nanoplatelets [14]. In order to analyse the effects of the orientation

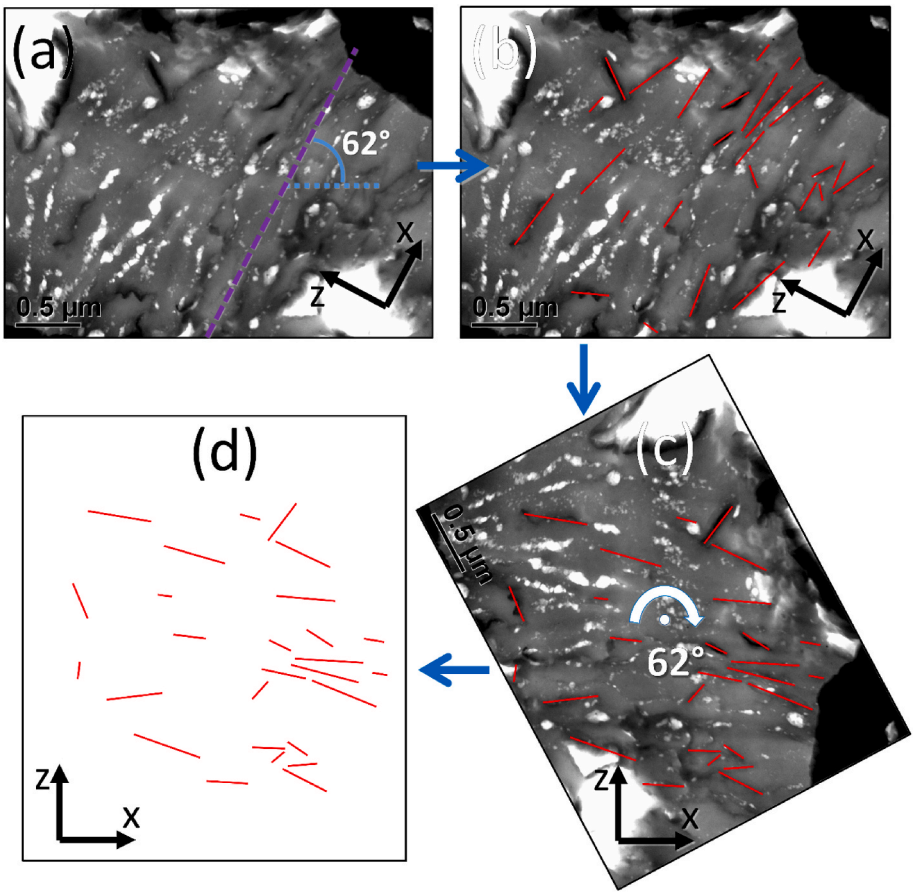

Fig. 7. Stages used for determination and highlighting of GNPs for 2.5 wt% GO-SA nanocomposite.

distribution of the nanoplatelets with the analytical models, the Krenchel orientation factor (η_o) [23] was implemented in the MROM, Hui-Shia, and Halpin-Tsai models in the following form:

$$E_{c,MRoM} = E_m v_m + \eta_{mrf}\eta_o E_f v_f \tag{1}$$

$$E_{c,Halpin-Tsai} = E_m \frac{1+\eta_o\eta_L v_f \xi}{1-\eta_o\eta_L v_f} \tag{2}$$

$$E_{c,Hui-Shia} = \frac{E_m}{1-\eta_o \frac{v_f}{4}\left[\frac{1}{\xi}+\frac{3}{\xi+\Lambda}\right]} \tag{3}$$

where the terms can be found in Ref. [14] with further details, while the Krenchel orientation factor used as described in Ref. [5]:

$$\eta_o = \frac{8}{15} + \frac{8}{21}\langle P_2(\cos\theta)\rangle + \frac{3}{35}\langle P_4(\cos\theta)\rangle \tag{4}$$

where $P_2(\cos\theta)$ and $P_4(\cos\theta)$ are Legendre polynomials:

$$P_2(\cos\theta) = \frac{1}{2}\left(3\cos^2\theta - 1\right) \tag{5}$$

$$P_4(\cos\theta) = \frac{1}{8}\left(35\cos^4\theta - 30\cos^2\theta + 3\right) \tag{6}$$

3. Results and discussion

When the TEM grids were observed with optical microscopy, some of the nanocomposite sections were found partially detached from the surrounding epoxy frames; an example of this is given in Fig. 3. Depending on the level of detachment, the sections wrinkled and/or partially folded over, i.e., the higher the level of detachment, the more extensive the process of wrinkling and folding over. Those types of artefacts were a problem in microscopic studies and reported numerous times in the literature [32,33].

The level of detachment is higher in sections (a) and (c) in the figure; it is lower for section (b). The sections normally have a thickness of ~50 μm (see Fig. 1 (f)). However, due to the partial detachment from the surrounding epoxy, and the folding-wrinkling behaviour, they appeared thinner (25–40 μm) on the grids. The red and purple lines show the z-axis (the short edge) and the x-axis (the long edge), respectively. The wrinkling and folding artefacts were mostly parallel to the long edge (x-axis or the plane of the nanocomposites) of the sections. Locations of folds nearly parallel to each other were also discussed in another source [33]. Therefore, the wrinkling and folding artefacts were used to support the axis-determination stage of the methodology developed in this study.

More than five sections were collected on the grids during the ultramicrotomy. However, most of the sections started to deteriorate due to the electron-beam damage in TEM. Only two sections could be successfully observed, one for each nanocomposite (Figs. 4 and 5). Micrographs of those sections were taken at various magnifications. The observation process of micrographs had to be swift in order to lessen the beam-exposure time. At least four different magnification ranges were used to correlate the micrographs with each other (images (c), (d), (e), (f) of Figs. 4 and 5): the smallest-scale micrographs show the GNP distributions; the largest scale micrographs show the orientations of the full sections. This allowed establishing a correlation between the orientation of the sections and orientation of the nanoplatelets.

When the full sections (refer to the brightened micrographs (b) in Figs. 4 and 5) were observed carefully, fold-over artefacts could be easily noticed. The artefacts, similar to their appearance in the OM images

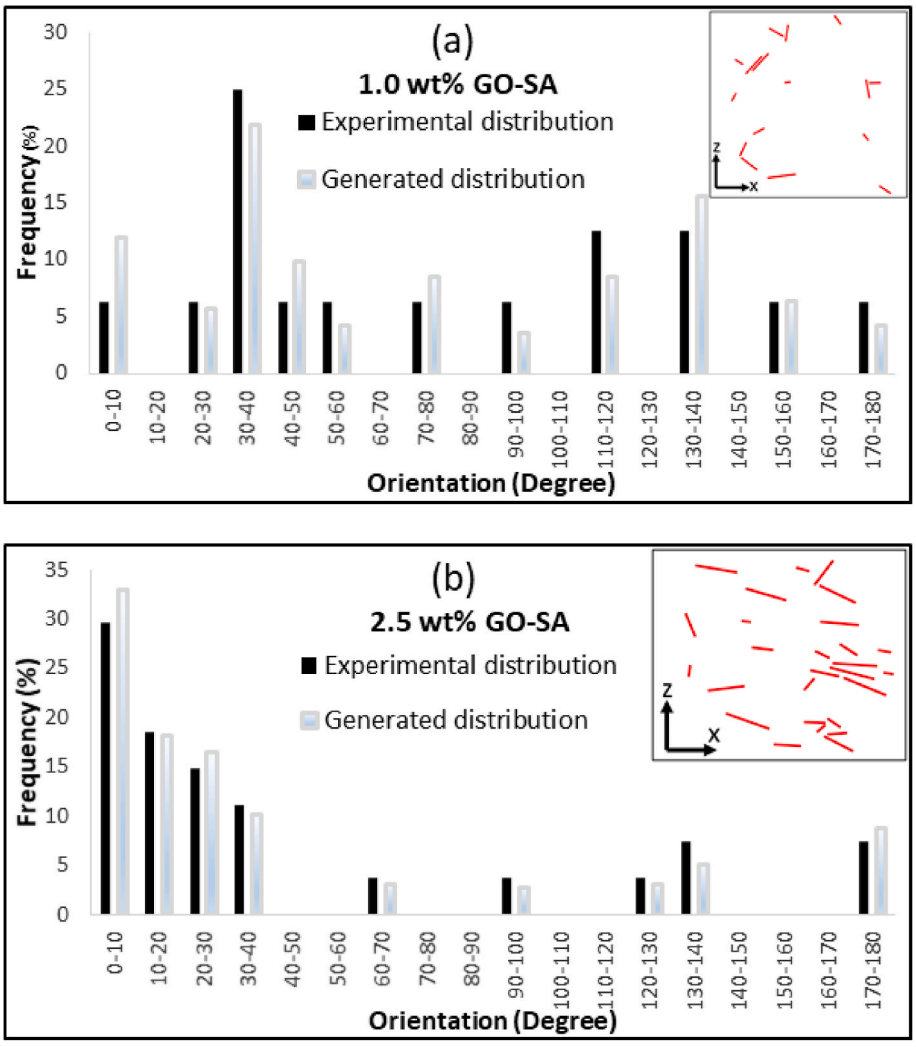

Fig. 8. Experimentally quantified distribution (dark bars) and generated distribution (gradient light blue bars) of GNPs for studied nanocomposites: (a) 1.0 wt% GO-SA; (b) 2.5 wt% GO-SA. The inner images depict the representative distributions used for analysis.

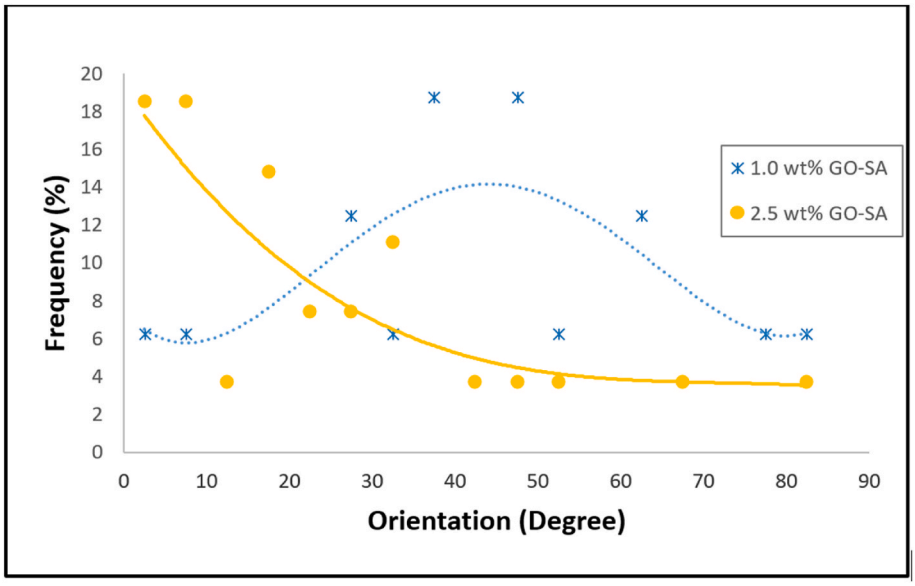

Fig. 9. Experimentally quantified distributions (markers) of GNPs with respective fitted curves (lines) in 0°–90° range for studied nanocomposites.

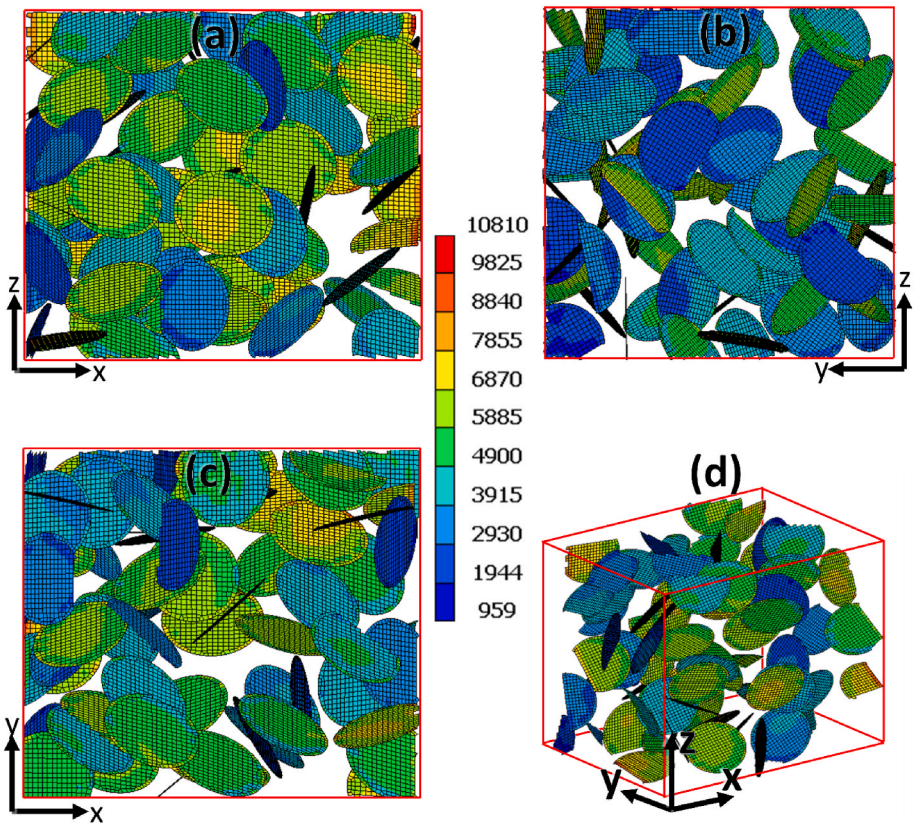

Fig. 10. Von Mises stress (in MPa) distributions on GNPs of the FE model of 1.0 wt% GO-SA nanocomposite for three different plane views (a, b, c) and isometric view (d) (A stress range bar is in the middle of the figure. The RVE had an edge size of 7.6 μm and the FE size was 200 nm).

(Fig. 3), appeared darker compared to the non-folded areas because the folded areas absorb relatively more photons and electrons. The 1.0 wt% GO-SA nanocomposite (Fig. 4 (b)) had more fold-overs compared to the 2.5 wt% one (Fig. 5 (b)). Similar to the preliminary findings from the OM work discussed in the methodology section, the higher the degree of fold-overs, the lower the appearance of the thickness (through-thickness, z-direction) of the sections. Therefore, the section of 2.5 wt% GO-SA nanocomposite looked thicker compared to that of 1.0 wt% GO-SA nanocomposite.

Edge detection of the top and bottom planes of the sections was performed based on their status. As the 2.5 wt% GO-SA nanocomposite section had fever artefacts, its edges were noticed relatively easily. However, the section's edges at another composite were more ambiguous. In that case, the fold-over lines (green in Fig. 4) were used to determine the parallelism of the section's plane. Based on that parallel, the top and bottom edges were predicted (purple lines). Between these edge lines, an orthogonal line (red) was plotted. A coordinate axis was assigned based on the edge (purple) lines and the through-thickness (red) line. By doing so, the planes of the 1.0 wt% and 2.5 wt% GO-SA nanocomposite sections were identified to have angles of 83° and 62°, respectively, to the horizontal line (micrographs (b) in Figs. 4 and 5).

The smallest-scale micrographs (micrographs (f) in Figs. 4 and 5) were also assigned the same local coordinate axis as their larger scale counterparts. The micrographs were rotated by the obtained angles in order to reorient them to their original positions (parallel to the horizontal line). Due to the low contrast in the micrographs (micrographs (a) in Figs. 6 and 7), they were assessed visually in order to detect and highlight GNPs that appear in the form of lines (micrographs (b) in Figs. 6 and 7). As the cross-section of a platelet is a line, such lines were analysed. Some platelets were preferentially aligned towards the x-z plane. A number of such GNPs was higher in the section of the 1.0 wt% GO-SA sample. It was probably due to the fact that the GNPs had more room to orient randomly when their number was low. The platelets in the x-z plane were exempted from the analysis, as their orientation was impossible to determine from the micrographs. After reorienting the micrographs and highlighting the GNP lines (micrographs (c) in Figs. 6 and 7), the original micrograph images were deleted, and the lines were enclosed in rectangular areas (Fig. 6 (d) and Fig. 7 (d)).

The obtained images (Fig. 6 (d) and Fig. 7 (d)) were processed with the *Nonwovens Anisotropy V1* software. The software assigns a starting point and an end point for each line (The former is assigned to the left end of the line and the latter to the right end). A vector was built from the starting point to the end point for each line. The vector's orientation was calculated with respect to the plane of the nanocomposite (x-y plane). The orientations were assigned in the angle range from 0° to 180°. The orientation distributions of the GNPs were quantified with probability density for GNPS as a function of their angular intervals (see the *experimental distributions* in Fig. 8). As can be seen from the experimental distributions, the increase in the fraction of GNPs led to a higher extent of their preferential alignment towards the main plane of the nanocomposites. This fact was presented and discussed qualitatively in previous papers that characterised the orientations based on transmission electron microscopy [6,13,14].

To calculate the ODFs of the GNPs, the orientation distributions were converted from 0° to 180° interval to 0°–90° interval. The distributions were plotted in form of frequency graphs (in %) as a function of degree in Fig. 9. The respective ODFs for 1.0 wt% GO-SA and 2.5 wt% GO-SA were calculated from the curve fitting of the raw data as follows:

$$f(\theta) = 4.8 \times 10^{-6}\theta^4 - 8.4 \times 10^{-4}\theta^3 + 0.0427\theta^2 - 0.509\theta + 7.53 \quad (7)$$

$$f(\theta) = -4 \times 10^{-5}\theta^3 + 0.0087\theta^2 - 0.636\theta + 19.33 \quad (8)$$

In order to assess the effectiveness of this quantification method, the finite-element technique was implemented in this study. In this respect,

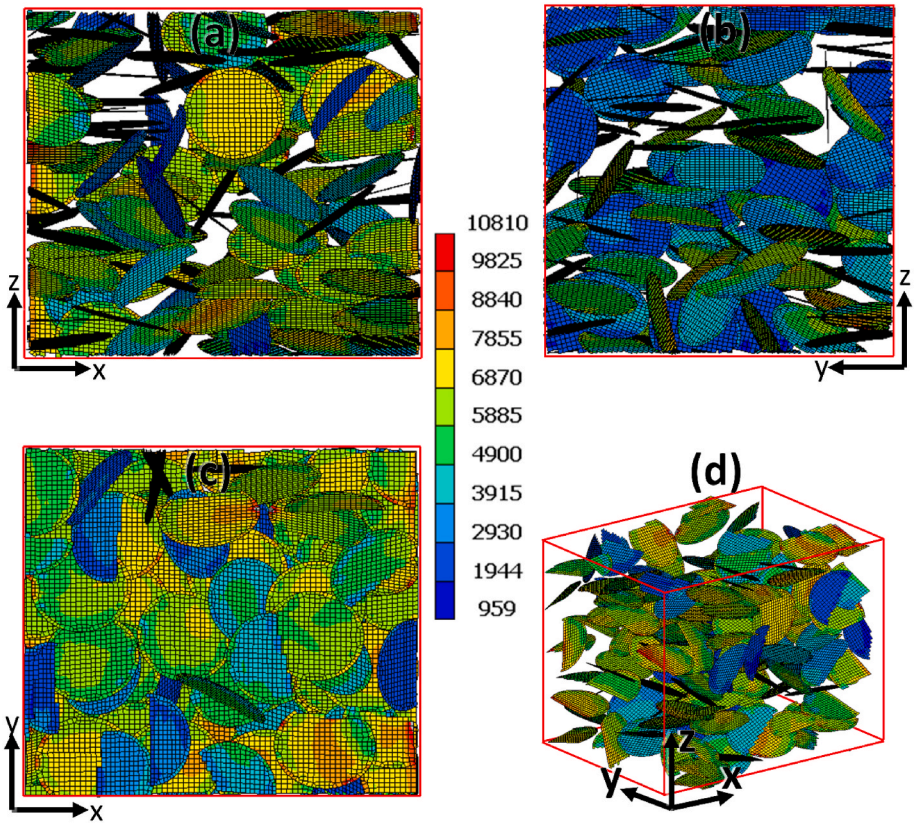

Fig. 11. Von Mises stress (in MPa) distributions on GNPs of the FE model of 2.5 wt% GO-SA nanocomposite for three different plane views (a, b, c) and isometric view (d) (The stress range bar is in the middle of the figure. The RVE had an edge size of 7.6 μm and the FE size was 200 nm).

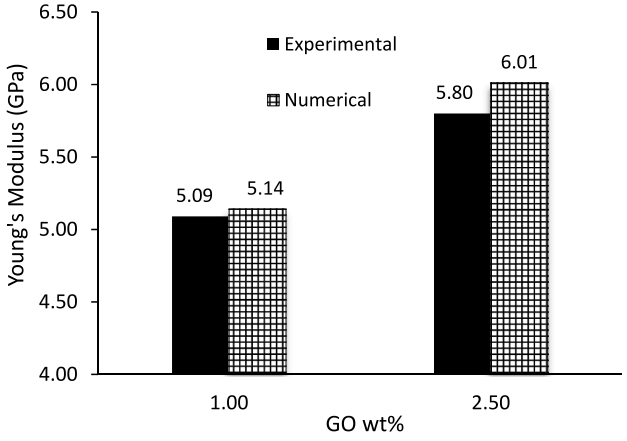

Fig. 12. Comparison of experimental and numerical results for Young's modulus of studied nanocomposite.

three-dimensional random spatial distribution of disks representing GNPs were generated based on the experimentally quantified distributions for different RVE sizes. For clarity, only one random distribution for each nanocomposite is presented in Fig. 8; other diagrams had a similar shape.

Analysis of mesh convergence and RVE size sensitivity were performed for the 1.0 wt% GO-SA nanocomposite. FE models with different mesh sizes were created in order to perform the mesh-convergence study. The elements with edge sizes of approximately 400 nm, 300 nm, 200 nm, and 150 nm were applied for the same RVE for this purpose. The maximum tensile load was recorded for each model. They were 26.1, 26.2, 26.1 and 26.05 mN, respectively. The discrepancies in the maximum loads were negligible. However, the stress gradients on the GNPs were smooth for models with 200 nm and 150 nm element sizes, while the rest had rough stress-gradient distributions. Therefore, an element edge size of 200 nm was chosen to mesh the nanocomposite models. RVE edge sizes of 3.1 μm, 5.3 μm, 7.6 μm, and 8 μm resulted in the effective Young's moduli of the nanocomposite of 5.14 GPa, 5.18 GPa, 5.11 GPa, and 5.14 GPa, respectively. This finding shows that the RVEs of all sizes exhibited consistent mechanical behaviour. As mesh convergence and RVE-size-sensitivity analyses yielded consistent results for the 1.0 wt% GO-SA nanocomposite, they were not performed for 2.5 wt% GO-SA nanocomposite. According to Ref. [34], RVE sizes that included more than 30 nanoclay platelets were insensitive to the RVE size. However, the FE models developed in our study were so consistent in their mechanical behaviour that they were insensitive to the RVE size down to a scale with only 5 nanoplatelets (RVE size 3.1 μm). Nonetheless, in order to make our study consistent with the literature with regard to the RVE-size selection, the RVE size of 7.6 μm was chosen, with the RVE containing about 71 and 149 nanoplatelets for 1.0 wt% GO-SA and 2.5 wt% GO-SA nanocomposites, respectively.

The FE models were stretched to the same magnitudes (1 %). Due to the different weight fractions and orientation distributions of the nanoplatelets, the maximum reaction forces obtained were different, 26 mN and 31 mN, respectively. The resultant stress distributions on the GNPs are depicted in Figs. 10 and 11. Von Mises stresses ranged from 1 GPa to 10 GPa. According to the literature, single-layer GO sheets with hole defects were estimated to have yield strength of some 30 GPa [35]. As the GNPs in our nanocomposites were intercalated structures of GO and SA layers, even when the yield strength of SA layers was neglected, GNPs would have yield strength higher than 15 GPa based on the Voigt's Rule of Mixtures (the volume fraction of GO in our GNPs were higher

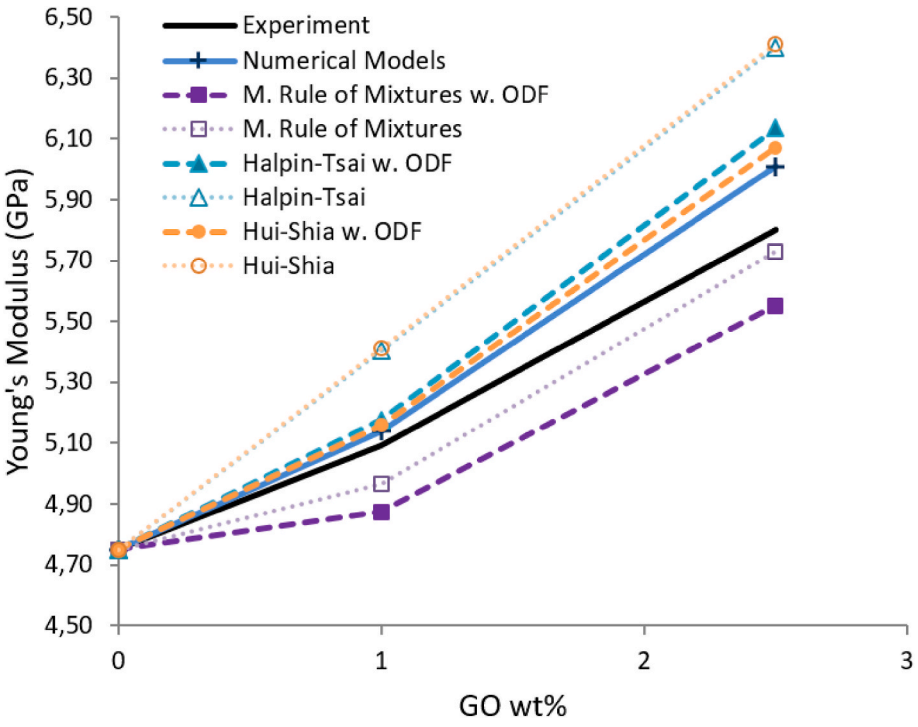

Fig. 13. *Comparison of ODF-modified analytical models with previously obtained analytical models (dotted lines [14]) as well as experimental and numerical results.*

than that in Ref. [14]). Therefore, according to FE, none of the GNPs would undergo plastic deformation at this strain level. GNPs that were better aligned towards the loading direction experienced higher stresses. As the number of preferentially aligned GNPs was higher in the 2.5 wt% GO-SA nanocomposites, the number of GNPs in high-stress ranges was greater in its FE model. The values of Young's moduli were calculated for both model; their experimental data were obtained from Ref. [14]. The experimental data and numerical results are compared in Fig. 12. The discrepancy between the results was highest for the nanocomposite with the higher fraction of GO; it was less than 4 %. For the nanocomposite with the lower fraction of GO, it was only about 1 %. It is well-known that as the GNP content increases in nanocomposites, so does the agglomeration rate [36,37]. The micrographs in this study do not indicate obvious agglomerations. This might be mainly due to the fact that the GO nanosheets formed intercalated morphologies of GNPs [14], which significantly reduced the number of inclusions in the matrix (as discussed above, the developed micromechanical models took the intercalated morphologies into account). A low number of inclusions potentially reduced the likelihood of further agglomerations. However, a slightly higher non-uniformity of spatial distribution of the GNPs was observed for the nanocomposites with their higher fraction. Therefore, the higher discrepancy for the nanocomposite with 2.5 wt% of GO might be due the non-uniformity of the spatial distributions that was not taken into account in the microstructural characterisation and modelling stages of our study.

The analytical micromechanics models were modified to incorporate the orientation distributions of the nanoplatelets. The Krenchel orientation factors (η_o) were calculated as 0.84 and 0.65 for 1.0 wt% and 2.5 wt% nanocomposites, respectively. The Young's modulus of the nanocomposites was calculated using Eqs. (1)–(3) and compared with the previous analytical results, in which the orientation distributions were not taken into account. Also, the numerical and the experimental findings were compared with the analytical results (Fig. 13). The ODF-modified Halpin-Tsai and Hui-Shia models were found to approximate the experimental results better than the ODF-modified MRoM approach. The numerical models still performed the best compared to all other models.

4. Conclusions

In this study, it was shown that the quantitative characterisation of orientation distribution of GNPs with respect to the surface plane of the nanocomposites can be successfully achieved with transmission electron microscopy. This is the first study proving it. Even though the number of micrographs that could have been acquired and analysed was low, the quantitative characterisation performed was of good accuracy, verified by experimental analysis and numerical simulations of the nanocomposites. A discrepancy of 1–4% between the stiffnesses was attributed to some neglected morphological features of graphene, such as waviness, irregular planar dimensions, and non-uniformity of spatial distribution of the nanoplatelets. Still, an accuracy of more than 95 % justifies the validity of the suggested method for quantitative characterisation of orientation distribution of graphene in nanocomposites using electron microscopy.

Halpin-Tsai and Hui-Shia micromechanical models were shown to perform better with modification accounting for the ODF while the MRoM performed less accurate with the ODF consideration. The developed numerical models approximated the experimental findings better than the analytical schemes.

The methods applied in this study are independent of the type of polymer matrix of the nanocomposites. Therefore, it can be concluded that the developed methodology can be implemented reliably for many types of GNP-reinforced polymer nanocomposites. For instance, the suggested methodology holds the potential to be implemented on nanocomposites reinforced with other types of nanoplatelets such as MXene and boron nitride. Application of the methodology suggested here would support the development and optimization studies of the nanocomposites.

The developed methodology was based on ultramicrotomy-sectioned samples. With the advent of new sample-preparation techniques of FIB and ultramicrotomy, and with the advances in TEM instruments [38], the suggested methodology can be further improved. The advancements would cover the most critical limitation of this study, which is burning of the nanocomposite sections under the TEM beams. A future work to overcome this limitation is planned.

The developed methodology is summarized below in the form of steps in order to help the researchers who would like to implement it in their studies. These steps do not cover every single detail of the TEM process, rather making some additions to the conventional approach, while some usual steps are not emphasized.

The methodology is as following.

- Prepare the nanocomposite in a film shape. If it has a bulk form, thin it down to thickness preferably below 100 μm.
- Assign the orthogonal axes for the film, e.g., x-axis (length), y-axis (depth), z-axis (thickness), x-y plane (plane of the film).
- Cut a pointed piece out of the film nanocomposite.
- Place the film in an embedding capsule. Make sure the x-y plane of the film is positioned nearly parallel to the main axis of the capsule; the pointed end is placed at the pointed end of the capsule and the film maintains a flat plane.
- Fill the capsule with resin and allow some time for curing.
- Trim the tip of the mould down to a geometry where the lateral dimension (x-axis) is at least five times larger than the thickness (z-axis) of the film.
- Cut the sections with a predefined thickness and mount them on a TEM grid.
- Study the grid-mounted sections with transmitted light optical microscopy in order to note dimensions and artefacts of the sections.
- Study the grids with a TEM at an optimum accelerating voltage.
- Start getting images from a low-magnification range, where the section dimensions are distinguishable, moving to a high-magnification range, where the nanoplatelets' cross-sections can be realized, keep the track of the relation between the parts of micrographs.
- Determine the x and z axes of the sections based on the orthogonal dimensions of the film's cross-section, i.e., its long edges and short edges corresponding to x-axis and z-axis, respectively. If the edges are not recognizable, refer to the artefacts that might appear parallel to the long edge of the section.
- Once the x- and z-axis assignment of the section is achieved, calculate the angle the x-axis of the section makes to the horizontal line.
- Rotate the section micrograph to bring its x-axis parallel to the horizontal line.
- If the contrast of the nanoplatelet cross-sections is poor, highlight them with lines.
- Apply image processing in order to determine the orientation distribution of the nanoplatelets.

CRediT authorship contribution statement

Osman Bayrak: Writing – original draft, Validation, Methodology, Investigation, Formal analysis, Conceptualization. **Mikhail Tashkinov:** Writing – original draft, Software, Methodology, Formal analysis. **Vadim V. Silberschmidt:** Writing – review & editing, Supervision, Conceptualization. **Emrah Demirci:** Writing – review & editing, Supervision, Conceptualization.

Declaration of competing interest

The authors declare that they have no known competing financial interests or personal relationships that could have appeared to influence the work reported in this paper.

Acknowledgements

The authors are grateful to Prof. Mariana Ionita from University Politehnica of Bucharest, Romania for supplying the nanocomposites, to Nicola Weston from NMRC, UK for the ultramicrotomy process and to Dr Zhaoxia Zhou from MCC Loughborough University, UK for operation of the TEM instrument. Dr Mikhail Tashkinov acknowledges the research project no. FSNM-2024-0013.

Data availability

Data will be made available on request.

References

[1] A.M. Sadoun, I.M.R. Najjar, M.S. Abd-Elwahed, A. Meselhy, Experimental study on properties of Al–Al2O3 nanocomposite hybridized by graphene nanosheets, J. Mater. Res. Technol. 9 (2020) 14708–14717, https://doi.org/10.1016/j.jmrt.2020.10.011.

[2] A. Fathy, A. Abu-Oqail, A. Wagih, Improved mechanical and wear properties of hybrid Al-Al2O3/GNPs electro-less coated Ni nanocomposite, Ceram. Int. 44 (2018) 22135–22145, https://doi.org/10.1016/j.ceramint.2018.08.326.

[3] O. Bayrak, M. Ionita, E. Demirci, V.V. Silberschmidt, Optical properties of graphene-based materials in transparent polymer matrices, Appl. Phys. Lett. 109 (2016), https://doi.org/10.1063/1.4961674.

[4] H. Liu, L.C. Brinson, Reinforcing efficiency of nanoparticles: a simple comparison for polymer nanocomposites, Compos. Sci. Technol. 68 (2008) 1502–1512, https://doi.org/10.1016/j.compscitech.2007.10.033.

[5] Z. Li, R.J. Young, N.R. Wilson, I.A. Kinloch, C. Vallés, Z. Li, Effect of the orientation of graphene-based nanoplatelets upon the Young's modulus of nanocomposites, Compos. Sci. Technol. 123 (2016) 125–133, https://doi.org/10.1016/j.compscitech.2015.12.005.

[6] B. Strommer, D. Schulze, B. Schartel, M. Böhning, The quantification of anisotropy in graphene/natural rubber nanocomposites: evaluation of the aspect ratio, concentration, and crosslinking, J. Appl. Polym. Sci. 140 (2023), https://doi.org/10.1002/app.53753.

[7] G. Dai, L. Mishnaevsky, Graphene reinforced nanocomposites: 3D simulation of damage and fracture, Comput. Mater. Sci. 95 (2014) 684–692, https://doi.org/10.1016/j.commatsci.2014.08.011.

[8] V.P. Matveenko, M.A. Tashkinov, Modeling the influence of structure morphology on the physical and mechanical properties of nanocomposites based on a polymer matrix and graphene oxide, Mech. Solid. 55 (2020) 316–323, https://doi.org/10.3103/S0025654420030097.

[9] O. Tapasztó, L. Tapasztó, H. Lemmel, V. Puchy, J. Dusza, C. Balázsi, K. Balázsi, High orientation degree of graphene nanoplatelets in silicon nitride composites prepared by spark plasma sintering, Ceram. Int. 42 (2016) 1002–1006, https://doi.org/10.1016/j.ceramint.2015.09.009.

[10] J.A. King, D.R. Klimek, I. Miskioglu, G.M. Odegard, Mechanical properties of graphene nanoplatelet/epoxy composites, J. Compos. Mater. 49 (2015) 659–668, https://doi.org/10.1177/0021998314522674.

[11] O.M. Kwon, H. Watanabe, K.H. Ahn, S.J. Lee, Growths of mechanical elasticity and electrical conductance of graphene nanoplatelet/poly(lactic acid) composites under strong electric field: correlation with time evolution of higher order structure of graphene nanoplatelets, Rheol. Acta 56 (2017) 871–885, https://doi.org/10.1007/s00397-017-1042-z.

[12] C. Dyer, K. Gkaliou, P. Anderson, C. Harrison, M. Eaton, J. Hall, Computer-controlled electromagnetic control and image capture system for alignment of magnetic graphene nanofillers in epoxy composites, Int. J. Appl. Electromagn. Mech. 61 (2019) S23–S29, https://doi.org/10.3233/JAE-192083.

[13] H. Kim, C.W. Macosko, Processing-property relationships of polycarbonate/graphene composites, Polymer 50 (2009) 3797–3809, https://doi.org/10.1016/j.polymer.2009.05.038.

[14] O. Bayrak, M. Ionita, E. Demirci, V.V. Silberschmidt, Effect of morphological state of graphene on mechanical properties of nanocomposites, J. Mater. Sci. 51 (2016) 4037–4046, https://doi.org/10.1007/s10853-016-9722-0.

[15] Z. Li, L. Deng, I.A. Kinloch, R.J. Young, Raman spectroscopy of carbon materials and their composites: graphene, nanotubes and fibres, Prog. Mater. Sci. 135 (2023), https://doi.org/10.1016/j.pmatsci.2023.101089.

[16] Z. Li, R.J. Young, I.A. Kinloch, N.R. Wilson, A.J. Marsden, A.P.A. Raju, Quantitative determination of the spatial orientation of graphene by polarized Raman spectroscopy, Carbon N. Y. 88 (2015) 215–224, https://doi.org/10.1016/j.carbon.2015.02.072.

[17] J. Mayer, L.A. Giannuzzi, T. Kamino, J. Michael, TEM sample preparation and FIB-induced damage, MRS Bull. 32 (2007) 400–407, https://doi.org/10.1557/mrs2007.63.

[18] G.J.C. Carpenter, Image and diffraction pattern rotations in the TEM, Micros, Today Off. 20 (2012) 52–55, https://doi.org/10.1017/s1551929512000697.

[19] D. Brandon, W. Kaplan, Microstructural Characterisation of Materials, Wiley-VCH Verlag, 2008, https://doi.org/10.1002/9780470727133.

[20] L. Yougui, Practical electron microscopy and database. www.globalsino.com/EM, 2006.

[21] Q. Chen, C. Dwyer, G. Sheng, C. Zhu, X. Li, C. Zheng, Y. Zhu, Imaging beam-sensitive materials by electron microscopy, Adv. Mater. 32 (2020), https://doi.org/10.1002/adma.201907619.

[22] E. Demirci, M. Acar, B. Pourdeyhimi, V.V. Silberschmidt, Computation of mechanical anisotropy in thermally bonded bicomponent fibre nonwovens, Comput. Mater. Sci. 52 (2012) 157–163, https://doi.org/10.1016/j.commatsci.2011.01.033.

[23] H. Krenchel, Fibre Reinforcement, Akademisk Forlag, Copenhagen, 1964.

[24] M. Ionita, M.A. Pandele, H. Iovu, Sodium alginate/graphene oxide composite films with enhanced thermal and mechanical properties, Carbohydr. Polym. 94 (2013) 339–344, https://doi.org/10.1016/j.carbpol.2013.01.065.
[25] X. Lu, F. Detrez, J. Yvonnet, J. Bai, Identification of elastic properties of interphase and interface in graphene-polymer nanocomposites by atomistic simulations, Compos. Sci. Technol. 213 (2021), https://doi.org/10.1016/j.compscitech.2021.108943.
[26] J.U. Lee, D. Yoon, H. Cheong, Estimation of Young's modulus of graphene by Raman spectroscopy, Nano Lett. 12 (2012) 4444–4448, https://doi.org/10.1021/nl301073q.
[27] O.L. Blakslee, D.G. Proctor, E.J. Seldin, G.B. Spence, T. Weng, Elastic constants of compression-annealed pyrolytic graphite, J. Appl. Phys. 41 (1970) 3373–3382, https://doi.org/10.1063/1.1659428.
[28] C. Lee, X. Wei, J.W. Kysar, J. Hone, Measurement of the elastic properties and intrinsic strength of monolayer graphene, Science 321 (2008) 385–388, https://doi.org/10.1126/science.1157996.
[29] J.W. Suk, R.D. Piner, J. An, R.S. Ruoff, Mechanical Properties of Monolayer Graphene Oxide, vol. 4, 2010, pp. 6557–6564.
[30] B. Raju, S.R. Hiremath, D. Roy Mahapatra, A review of micromechanics based models for effective elastic properties of reinforced polymer matrix composites, Compos. Struct. 204 (2018) 607–619, https://doi.org/10.1016/j.compstruct.2018.07.125.
[31] Y. Dong, D. Bhattacharyya, P.J. Hunter, Experimental characterisation and object-oriented finite element modelling of polypropylene/organoclay nanocomposites, Compos. Sci. Technol. 68 (2008) 2864–2875, https://doi.org/10.1016/j.compscitech.2007.10.026.
[32] H.H. Crowley, B.H. Leichtling, Elimination or reduction of wrinkles in semithin epoxy sections by vacuum drying, Biotech. Histochem. 64 (1989) 221–223, https://doi.org/10.3109/10520298909107004.
[33] A.B. Maunsbach, B.A. Afzelius, Biomedical Electron Microscopy: Illustrated Methods and Interpretations, Academic Press, 1999, https://doi.org/10.1016/B978-0-12-480610-8.X5000-8.
[34] K. Hbaieb, Q.X. Wang, Y.H.J. Chia, B. Cotterell, Modelling stiffness of polymer/clay nanocomposites, Polymer 48 (2007) 901–909, https://doi.org/10.1016/j.polymer.2006.11.062.
[35] J.T. Paci, T. Belytschko, G.C. Schatz, Computational studies of the structure, behavior upon heating and mechanical properties of graphite oxide, J. Phys. Chem. C 111 (2007) 18099–18111, https://doi.org/10.1021/jp075799g.
[36] Z. Li, J. Chu, C. Yang, S. Hao, M.A. Bissett, I.A. Kinloch, R.J. Young, Effect of functional groups on the agglomeration of graphene in nanocomposites, Compos. Sci. Technol. 163 (2018) 116–122, https://doi.org/10.1016/j.compscitech.2018.05.016.
[37] M.K. Hassanzadeh-Aghdam, Evaluating the effective creep properties of graphene-reinforced polymer nanocomposites by a homogenization approach, Compos. Sci. Technol. 209 (2021) 108791, https://doi.org/10.1016/j.compscitech.2021.108791.
[38] B. Kuei, M.P. Aplan, J.H. Litofsky, E.D. Gomez, New opportunities in transmission electron microscopy of polymers, Mater. Sci. Eng. R Rep. 139 (2020) 100516, https://doi.org/10.1016/j.mser.2019.100516.